JACC: BASIC TO TRANSLATIONAL SCIENCE VOL. 8, NO. 7, 2023

ORIGINAL RESEARCH - PRECLINICAL

Bioprosthetic Valve Deterioration

Accumulation of Circulating Proteins and Macrophages in the Valve Interstitium

Tomohisa Sakaue, PHD,[a,b] Tadaaki Koyama, MD, PHD,[c] Yoshitsugu Nakamura, MD, PHD,[d] Keitaro Okamoto, MD,[e] Takayuki Kawashima, MD,[e] Tadashi Umeno, MD,[e] Yasuhide Nakayama, PHD,[e,f] Shinji Miyamoto, MD, PHD,[e] Fumiaki Shikata, MD, PHD,[a] Mika Hamaguchi, MD,[g] Jun Aono, MD, PHD,[g] Mie Kurata, MD, PHD,[h,i] Kenji Namiguchi, MD,[a] Shunji Uchita, MD, PHD,[a] Junya Masumoto, MD, PHD,[h,i] Osamu Yamaguchi, MD, PHD,[g] Shigeki Higashiyama, PHD,[b,j,k] Hironori Izutani, MD, PHD[a]

VISUAL ABSTRACT

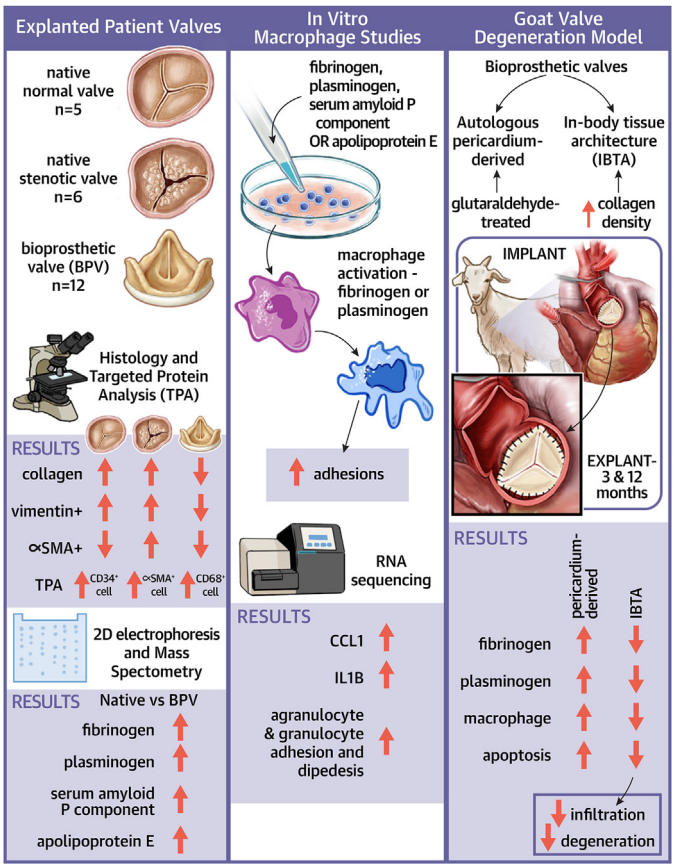

Sakaue T, et al. J Am Coll Cardiol Basic Trans Science. 2023;8(7):862-880.

HIGHLIGHTS

- We found crucial differences in cellular and collagen contents between the native and bioprosthetic valves.
- Proteomics uncovered an accumulation of blood proteins as a macrophage activator in the interstitial spaces.
- Excessive cell accumulations of apoptotic macrophages were found in the pericardium-derived bioprostheses.
- Structural improvements by increasing collagen density of bioprostheses are one of the effective anti-deterioration therapies.

From the [a]Department of Cardiovascular and Thoracic Surgery, Ehime University Graduate School of Medicine, Toon, Japan; [b]Department of Cell Growth and Tumor Regulation, Proteo-Science Center, Toon, Japan; [c]Department of Cardiovascular Surgery, Kobe City Medical Center General Hospital, Kobe, Japan; [d]Department of Cardiovascular Surgery, Chiba-Nishi General Hospital, Matsudo, Japan; [e]Department of Cardiovascular Surgery, Oita University, Yufu, Japan; [f]Biotube, Tokyo, Japan; [g]Department of

ISSN 2452-302X https://doi.org/10.1016/j.jacbts.2023.01.003

SUMMARY

Histologic evaluations revealed excessive accumulations of macrophages and absence of fibroblastic interstitial cells in explanted bioprosthetic valves. Comprehensive gene and protein expression analysis and histology unveiled an accumulation of fibrinogen and plasminogen, an activator of infiltrated macrophages, from degenerated valve surfaces in the interstitial spaces. These pathologies were completely reproduced in a goat model replaced with an autologous pericardium-derived aortic valve. Further preclinical animal experiments using goats demonstrated that preventing infiltration of macrophages and circulating proteins by increasing collagen density and leaflet strength is an effective treatment option. (J Am Coll Cardiol Basic Trans Science 2023;8:862–880) © 2023 The Authors. Published by Elsevier on behalf of the American College of Cardiology Foundation. This is an open access article under the CC BY-NC-ND license (http://creativecommons.org/licenses/by-nc-nd/4.0/).

ABBREVIATIONS AND ACRONYMS

APCS = anti-serum amyloid P component

APOE = apolipoprotein E

AS = aortic valve stenosis

AVR = aortic valve replacement

BV = bioprosthetic valve

CD = cluster of differentiation

CTSD = cathepsin D

eBV = explanted bioprosthetic valve

FGB = fibrinogen β-chain

IBTA = in-body tissue architecture

PLG = plasminogen

SMA = smooth muscle actin

Aortic valve bioprosthesis implantation is a suitable treatment for patients older than 60 years with aortic valve stenosis (AS). Patients do not require long-term anticoagulation therapy after the implantation of porcine or bovine bioprostheses,[1] and these valves contribute substantially to the acceleration of treatments for patients with aortic valve diseases. However, biological valves are occasionally explanted because of structural valve deterioration with calcification and valve thrombosis.[2] Previous clinical investigations have shown that structural valve deterioration was the most common reason for reoperation[3,4] and that the structural valve deterioration rates at 10 and 20 years after implantation were 1.9% and 15%, respectively.[5] Recently, with the increased number of patients with transcatheter-mediated bioprosthetic valves (BVs), leaflet thrombosis associated with BVs has been reported. Chakravarty et al[6] reported that subclinical leaflet thrombosis was observed in implanted surgical and transcatheter aortic BVs. However, the molecular mechanisms underlying BV degeneration remain unclear, and additional molecular-based investigations, such as molecular profiling analysis and detailed pathologic definition, are required to determine the optimal treatment or prevention of valve thrombosis and calcification.[7]

Our previous molecular-based case study of an explanted bioprosthetic valve(eBV) (Magna EASE, Medtronic) provided the first evidence that fibrinogen and plasminogen (PLG) were deposited onto degenerated calcified valve leaflets.[8] A recent study revealed that serum albumin infiltration contributes to BV degeneration,[9] indicating that pericardium-derived biological valves may easily allow circulating components' infiltration.

Here, we collected cases with multiple BV explantation and investigated the infiltrated cell types and differential patterns of protein expression in the native valves and BVs to elucidate the pathologic features and molecular profile of degenerated BVs. Additionally, we determined the molecular mechanism underlying structural valve deterioration with calcifications using pathologic and molecular biological techniques to develop antideterioration agents.

METHODS

PATIENT SELECTION AND SAMPLE PREPARATION. Stenotic native aortic valves were obtained from patients with AS who required aortic valve replacement (AVR), as previously reported.[8] Aortic BVs were explanted from another group of patients who also required AVR. Normal aortic valves were obtained from autopsy cases.[8] The valve leaflets were

Cardiology, Pulmonology, Hypertension, and Nephrology, Ehime University Graduate School of Medicine, Toon, Japan; [h]Department of Pathology, Division of Analytical Pathology, Ehime University Graduate School of Medicine, Toom, Japan; [i]Department of Pathology, Proteo-Science Center, Toon, Japan; [j]Department of Biochemistry and Molecular Genetics, Ehime University Graduate School of Medicine, Toon, Japan; and the [k]Department of Molecular and Cellular Biology, Research Center, Osaka International Cancer Institute, Osaka, Japan.

The authors attest they are in compliance with human studies committees and animal welfare regulations of the authors' institutions and Food and Drug Administration guidelines, including patient consent where appropriate. For more information, visit the Author Center.

Manuscript received March 2, 2022; revised manuscript received January 3, 2023, accepted January 3, 2023.

JACC: BASIC TO TRANSLATIONAL SCIENCE VOL. 8, NO. 7, 2023
JULY 2023:862–880

separated into 2 equal parts for western blot analysis and immunohistochemistry. The protein integrities or fragmentation during experimental treatments were evaluated using electrophoresis with Coomassie brilliant blue staining. The characteristics of the patients with native AS valves (n = 6), patients with BVs (n = 12), and autopsy cases (n = 5) are presented in Supplemental Tables 1 to 3, respectively. Sample collection and experimental flows are represented in Supplemental Figure 1. All experiments were approved by the Ehime University internal review board (protocols 1509022 and 1603002), and patients or their families provided written informed consent before experiments commenced.

REAGENTS AND ANTIBODIES. Anti-vimentin antibody (D21H3) XP rabbit monoclonal antibody (catalog #5741), anti-cathepsin D (CTSD) antibody (catalog #2284), cleaved caspase-3 (Asp175) (5A1E) rabbit monoclonal antibody (catalog #9664), and anti-cluster of differentiation 68 (CD68) (D4B9C) rabbit monoclonal antibody (catalog # 76437S) were obtained from Cell Signaling Technology. Anti-CD31 rabbit polyclonal antibody (catalog #ab28364) and anti-vimentin antibody (catalog#ab8979) were purchased from Abcam. Anti-α-smooth muscle actin (SMA) antibody was obtained from Novus Biologicals. Antifibrinogen β-chain (FGB) (catalog #HPA001900) and anti-PLG (catalog #HPA048823) antibodies were purchased from Sigma-Aldrich. Anti-CD34 (catalog #MCA547GT) monoclonal antibodies were obtained from Bio-Rad Laboratories. Anti-apolipoprotein E1 (APOE) (catalog #66830-l-lG) and anti-serum amyloid P component (APCS) (catalog #20773-1-AP) antibodies were purchased from Proteintech. Production of anti-goat PLG rabbit polyclonal antibodies were outsourced to SCRUM. The SYPRO Ruby Protein Gel Stain kit and Bio-Safe Coomassie blue stain solution were purchased from Thermo Fisher Scientific and Bio-Rad Laboratories, respectively. Preimplanted Freestyle aortic root and Magna EASE bioprostheses were purchased from Medtronic and Edwards Lifesciences, respectively.

HISTOLOGIC ANALYSIS. The histologic structure, extracellular matrix, and valve calcification were visualized using hematoxylin and eosin, Masson's trichrome, and von Kossa staining, respectively, as previously described.[8,10] Horseradish peroxidase-diaminobenzidine-based immunostaining using anti-FGB (1:10,000), PLG (1:10,000), APOE (1:10,000), APCS (1:10,000), CD68 (1:200), CTSD (1:200), and cleaved caspase-3 (Asp175) (1:200) and immunofluorescence staining with anti-CD34, CD68, FGB (1:200), PLG (1:200), APOE (1:200), APCS (1:200), CD68 (1:200), CTSD (1:200), and cleaved caspase-3 (Asp175) (1:200) were processed as previously described.[8] Briefly, peroxidase-conjugated anti-mouse and antirabbit IgG Histofine Simple Stain Max-PO (Nichirei Bioscience), and Goat anti-Mouse or Rabbit IgG (H+L) Cross-Adsorbed Secondary Antibody, Alexa Fluor™ 488 or 568 were used for DAB staining and immunofluorescence staining, respectively. Whole-valve views were obtained as tiled images using a BZ-X800 microscope (Keyence). High-magnification images were obtained using an A1R confocal laser microscope (Nikon).

SODIUM DODECYL SULFATE–POLYACRYLAMIDE GEL ELECTROPHORESIS AND WESTERN BLOTS. The explanted valve leaflets in the Laemmli sodium dodecyl sulfate sample buffer were homogenized using a Polytron homogenizer (model PT-10-35 GT). Subsequently, all proteins were extracted using the methanol-chloroform-water method. After measuring the protein concentration using the RC DC Protein Assay Kit (Bio-Rad),[11] 10 μg (for Coomassie blue staining), 1 μg (for western blotting with anti-FGB, PLG, APOE, and APCS antibodies), or 20 μg (for western blotting with anti-CD34, CD68, vimentin, and α-SMA antibodies) of proteins was subjected to sodium dodecyl sulphate-polyacrylamide gel electrophoresis. To visualize the proteins, the samples were stained with Bio-Safe Coomassie blue stain. For western blotting, the subjected protein bands were transferred to polyvinylidene difluoride membranes. After reactions with the primary antibodies (anti-FGB [1:2,000], anti-PLG [1:2,000], anti-APOE [1:2,000], anti-APCS [1:2,000], anti-CD34 [1:1,000], anti-vimentin [1:1,000], and anti-CD68 [1:1,000]), target proteins were indirectly visualized using horseradish peroxidase-conjugated antirabbit secondary antibodies (Promega; 1:4,000) and the Enhanced Chemiluminescence Prime Western Blotting Detection System (GE Healthcare Life Sciences).[12] Chemiluminescence images were obtained using the LAS-4000 luminescent image analyzer (Fujifilm Life Sciences USA).

TWO-DIMENSIONAL GEL ELECTROPHORESIS. Overall, 150 μg proteins were extracted from explanted native valves and BVs using a urea lysis buffer containing 8.5 mol/L urea, 0.2% Bio-Lyte 3/10 (Bio-Rad Laboratories), and 4% 3-[(3-cholamidopropyl)-dimethylammonium]-1-propanesulfonate (Dojin Laboratories). The proteins were separated on Immobiline DryStrip gels (length 130 mm, pH 3-10; GE Healthcare Life Sciences), followed by 12.5% sodium dodecyl sulphate-polyacrylamide gel electrophoresis. Protein bands were visualized using staining with Coomassie

blue. Gel images were acquired using the Image Scanner II (GE Healthcare Life Sciences).

MATRIX-ASSISTED LASER DESORPTION IONIZATION TIME OF FLIGHT/MASS SPECTROMETRY. Mass spectral analysis was performed to identify the protein bands.[8] The obtained spectra were analyzed using the Mascot search engine (Matrix Science) and against NCBIprot 20180429 (152,462,470 sequences, 55,858,910,152 residues).

CELL CULTURE AND CELL ADHESION ASSAY. A human monocytic leukemia cell line (THP-1, catalog # EC88081201-G0) from KAC was maintained in RPMI 1640 supplemented with 10% fetal bovine serum, streptomycin (100 μg/mL), and penicillin (20 U/mL). After culturing THP-1 with 50 ng/mL vitamin D3, 1α, 25-dihydroxy (Merck Millipore), the cells were incubated with 1 mg/mL fibrinogen (catalog #F3879, Sigma-Aldrich) or protein mixtures of fibrinogen (1 mg/mL), PLG (20 μg/mL; catalog #164-24271, Wako Pure Chemical Industries), APOE (1 μg/mL; catalog #SRP6303, Sigma-Aldrich), and APCS (1 μg/mL; catalog #1948-SAB) for 24 hours. The number of adhered THP-1 cells on the bottom of the culture dish was counted.

RNA SEQUENCING AND GENE ENRICHMENT ANALYSIS. Total RNA was isolated using Isogen II (NipponGene) according to the manufacturer's protocol. The RNA integrity number of the purified RNAs was evaluated using the Bioanalyzer RNA6000 Nano kit (Agilent Technologies). In particular, 300 ng RNA was subjected to RNA sequencing using the NEBNext Ultra Directional RNA Library Prep Kit for Illumina and NEBNext Poly(A) messenger RNA isolation kit (New England Bio Labs). Generated libraries were sequenced using the MiSeq Reagent Kit version 3 150-cycle kit on a MiSeq system (Illumina). Fragments per kilobase of exon per million fragments mapped read data were used for relative expression analysis. Visualizations of activated and inactivated signal pathways on the basis of the enriched genes were performed using Ingenuity Pathway Analysis software (Qiagen).

QUANTIFICATIONS OF MESSENGER RNAs. One microgram purified RNA was reverse transcribed using the High Capacity cDNA Synthesis Kit (Applied Biosystems) according to the manufacturer's protocol. SYBR green-based real-time quantitative polymerase chain reaction was performed using StepOne Plus real-time polymerase chain reaction system (Applied Biosystems). Relative gene expressions were calculated using the delta-delta method. The primers used in this study are presented in Supplemental Table 4.

ANIMAL EXPERIMENTS. All animal experiments in this study were approved by the Oita University Animal Ethics Committee (approval #1622001). Biosheet production and selection and the AVR procedure in goats were conducted, as previously described.[13] Briefly, Biosheets were produced by embedding molds in abdominal subcutaneous pouches in adult Saanen goats for 2 months, followed by harvesting and storing in a 70% ethanol solution until use. After left thoracotomy, the hearts were arrested, and native aortic valves were excised. The Biosheet-derived valves, trimmed according to the Ozaki procedure, were implanted in the aortic positions.

Conversely, the harvested pericardium was treated with a physiological salt solution-based 0.6% glutaraldehyde solution for 10 min. The rinsed pericardium was implanted in the aortic position. The goats were sacrificed under anesthesia, and each valve (Biosheet and autologous pericardium groups) was harvested. The Biosheet, pericardium, and native valve leaflets were used for histologic analyses and western blotting. The excised normal native leaflets were used as controls. A goat that died at 9 months after implantation of infective endocarditis was excluded. All goats used in this study are listed in Supplemental Table 5.

DETECTION OF APOPTOTIC CELLS. To visualize the apoptotic cells in the goat tissues, the DeadEnd Fluorometric TUNEL System (catalog #G3250, Promega) was used according to the manufacturer's protocol. Deparaffinized samples were fixed with 4% paraformaldehyde for 15 minutes, followed by digestion with proteinase K (20 μg/mL) for 10 minutes. After treatment with nucleotide mix and recombinant terminal deoxynucleotidyl transferase enzyme for 60 minutes at 37 °C, the nuclei were stained with Hoechst 33342. The fluorescent signals were visualized using an A1R confocal laser microscope. Quantifications of fluorescent signals were carried out using ImageJ software (National Institutes of Health).

STATISTICAL ANALYSES. All results are expressed as mean ± SEM. The normality of the obtained experimental data was assessed using the Shapiro-Wilk test. Comparisons between 2 groups were performed using Student's *t*-test, while comparisons among more than 2 groups was conducted using 1-way analysis of variance or the Kruskal-Wallis test for normally and non-normally distributed data, respectively. The Dunnett, Dunn, or Sidak post hoc method was used for multiple pairwise comparisons to adjust type I errors. The strength and direction of the linear association between 2 continuous variables were assessed using the Pearson correlation coefficient (*r*). Analyses

JACC: BASIC TO TRANSLATIONAL SCIENCE VOL. 8, NO. 7, 2023
JULY 2023:862–880

FIGURE 1 Sparse Collagen Fibers and Fewer Mesenchymal Cells in Bioprosthetic Valves

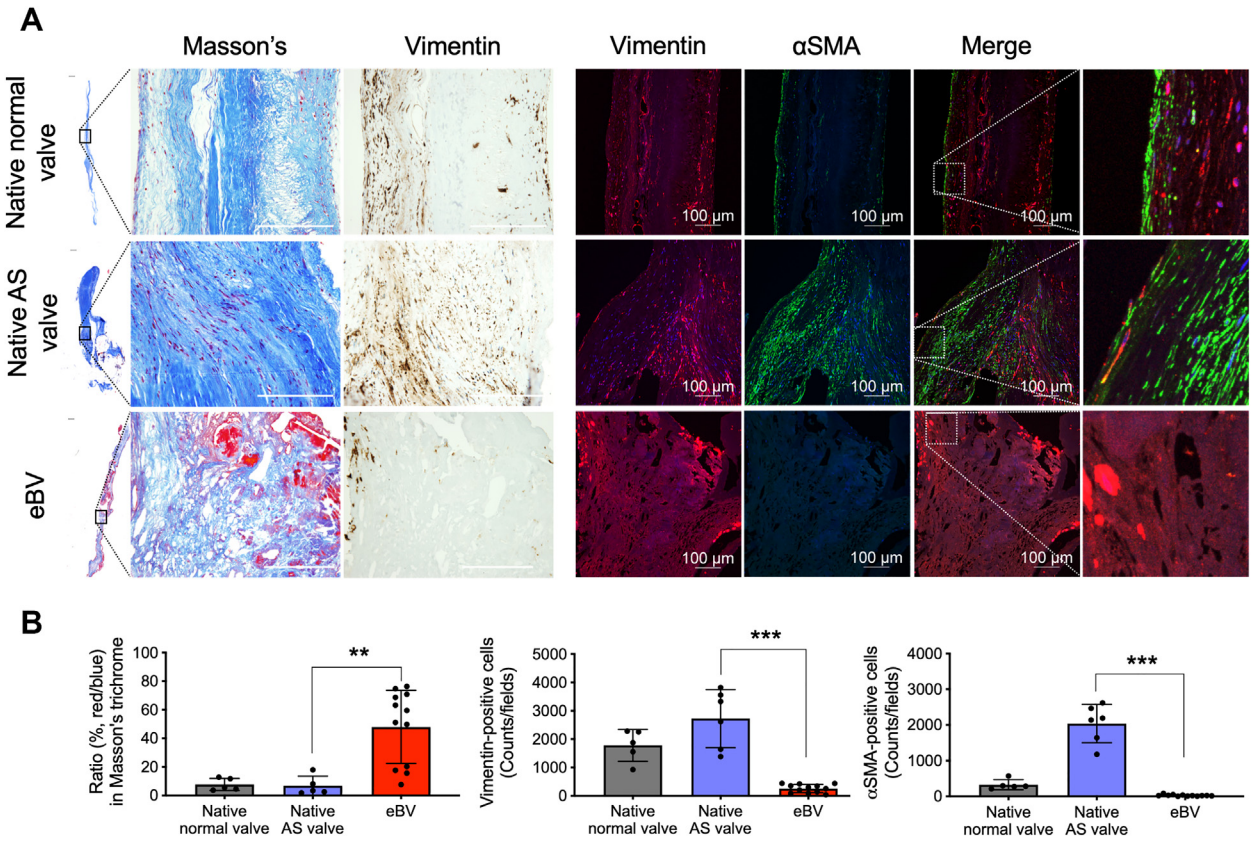

(A) Masson's trichrome staining and immunohistochemical staining for vimentin and anti-α-smooth muscle actin (SMA) of explanted bioprosthetic valves (eBVs) and normal native and aortic valve stenosis (AS) valves. The **left panels** are whole views of the valve leaflets. Scale bars, 100 μm. The **right panels** show colocalizations of vimentin and αSMA in the valves. **(B)** Quantitative data of the ratios (%) of red/blue areas of Masson's trichrome staining, vimentin-positive cells, and α-SMA-positive cells in the valves. Statistical analyses were performed using the Kruskal-Wallis test with Dunn's multiple-comparisons test (all comparisons). $^{**}P < 0.01$ and $^{***}P < 0.001$.

were conducted using Prism (GraphPad Software), and a P value <0.05 was considered to indicate statistical significance.

RESULTS

LOW CONTENT OF VIMENTIN-POSITIVE INTERSTITIAL CELLS AND SPARSE COLLAGEN FIBER NETWORKS IN eBVs. To clarify the histologic features of the eBVs, we collected preimplanted porcine or bovine BVs and eBVs from patients indicated for AVR (Supplemental Figure 2) and subsequently compared the hematoxylin and eosin-stained, von Kossa-stained, and Masson's trichrome-stained tissues of their bioprosthetic leaflets with those of the normal, preimplanted aortic valve leaflets (Supplemental Figure 3). Masson's trichrome staining (red/blue ratio [red, cytoplasm and fibrin; blue, elastic fiber]) showed that collagen fiber densities in native normal and AS valves were significantly higher than those in eBVs (**Figures 1A and 1B**). Moreover, accumulations of infiltrated blood components derived from the red color in Masson's trichrome staining were extensively observed in the interstitium of eBVs (**Figures 1A and 1B**). Three-layer and cellular architectures with vimentin-positive interstitial valve cells and surface localization of α-SMA-positive myofibroblasts were observed in normal aortic valve leaflets (**Figure 1A**). Although an abundance of vimentin-positive cells and α-SMA-positive myofibroblasts responsible for the production of collagen fibers was observed in the interstitium of the native AS valves, no myofibroblasts and significantly few vimentin-positive cells were detected in the tissue valves (**Figures 1A and 1B**, Supplemental Figure 4).

FIGURE 2 **Quantification and Localization Analysis of CD34-, αSMA-, and CD68-Positive Cells**

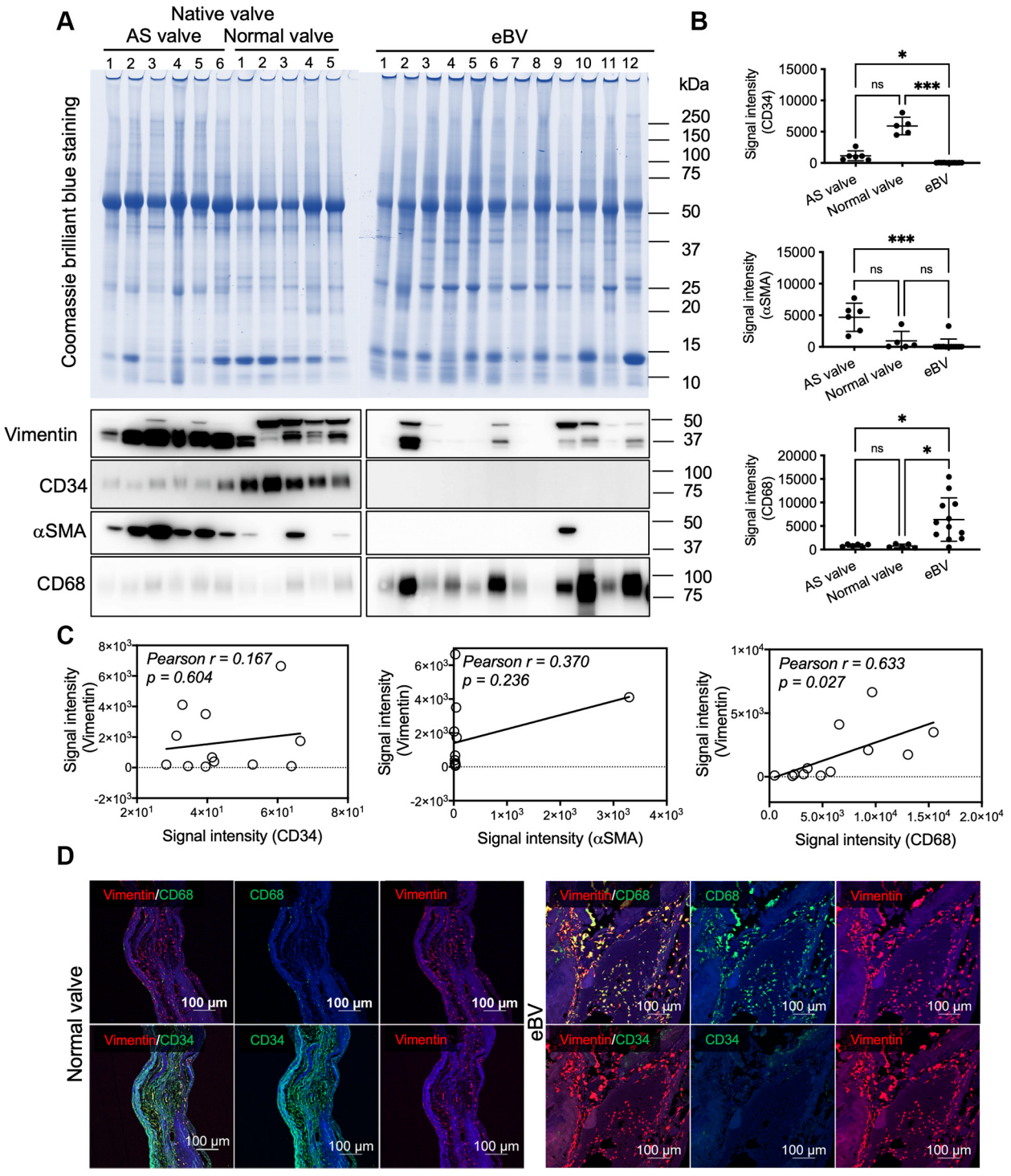

(A) The **upper panel** shows sodium dodecyl sulphate-polyacrylamide gel electrophoresis images of the tissue lysates (total protein 10 μg) from patients with AS (n = 6), normal (n = 5), and eBVs (n = 12). **(B)** Quantification and statistical analyses in western blotting of **(A)**. Kruskal-Wallis test and Dunn's multiple-comparisons test (all comparisons) were used to analyze the cluster of differentiation 34 (CD34), αSMA, and CD68 levels between the AS and normal native valves. *$P < 0.05$ and ***$P < 0.001$. **(C)** Correlations of the protein levels of vimentin and cell-specific markers (CD34, αSMA, and CD68). **(D)** Immunofluorescence costaining of vimentin/CD68 or vimentin/CD34 in the normal and bioprosthetic valves. Scale bars, 100 μm. Abbreviations as in Figure 1.

FIGURE 3 **Protein Profiling in Tissue Lysates From the Explanted Native Valves (AS and Normal) and eBVs**

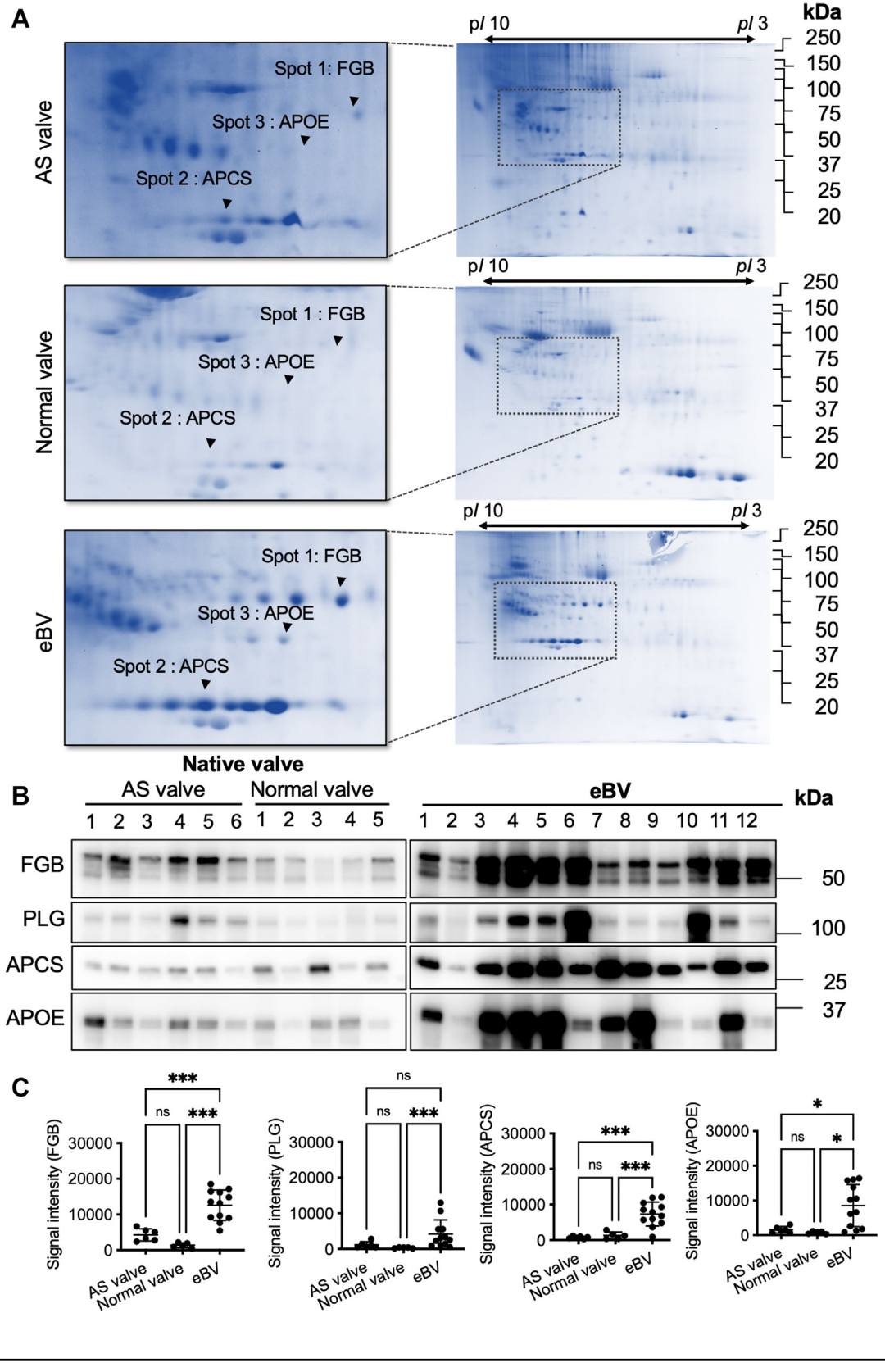

Continued on the next page

These data indicate critical differences in histologic features, including collagen contents, localization, and the number of vimentin-positive cells, between bioprosthetic and native valves.

CELL COMPOSITIONS OF EXPLANTED NATIVE VALVES AND BVs. To clarify and quantify the cell types of vimentin-positive cells in BVs, we extracted whole proteins from homogenized tissue lysates and quantitatively analyzed the expression levels of CD34 (for immature endothelial and fibroblastic cells), α-SMA (for myofibroblasts), and CD68 (for macrophages) using western blotting. To assess whether equal amounts of proteins extracted from the native and eBV tissues were loaded, we visualized all protein bands using Coomassie blue staining (**Figure 2A**). Although CD34 proteins were strongly expressed in lysates from the normal valves compared with the tissue valves, the CD34 protein levels tended to decrease in lysates from patients with AS (**Figures 2A and 2B**). Conversely, α-SMA was overexpressed in lysates from patients with AS rather than in lysates from normal valves (**Figures 2A and 2B**). However, both proteins were infrequently observed in lysates from eBVs (**Figures 2A and 2B**). CD68 overexpression was detected in lysates from eBVs, while low expression of CD68 was observed in lysates from native valves, with no significant difference between AS and normal valves (**Figures 2A and 2B**). A positive correlation (Pearson's $r = 0.633$; $P = 0.027$) between the expression levels of vimentin and those of CD68 was identified (**Figure 2C**). To confirm the western blot data, we evaluated the tissue distribution of CD34- and CD68-positive cells. CD34 and vimentin double-positive cells were widely located in the interstitium and on the surface of the normal valves but not in the eBVs (**Figure 2D**). CD68-derived fluorescence signals were detected in most vimentin-positive cells (**Figure 2D**), consistent with the western blot data (**Figure 2A**). Capillaries in the human heart tissues and paraffin-embedded THP-1 cells were used as positive controls in CD34 and CD68 immunofluorescence staining, respectively (Supplemental Figure 5). These data suggest that the accumulation of CD68-positive macrophages is specifically observed in degenerated bioprostheses.

ACCUMULATION OF CIRCULATING PROTEINS IN THE INTERSTITIUM. To clarify the differences in protein profiling between native valves and BVs, we conducted 2-dimensional gel electrophoresis and compared the protein profiles of the tissue lysates from the explanted, normal, and AS valves. We found 3 different proteins (48, 35, and 30 kDa) with high expression levels in eBVs lysates (**Figure 3A**). Three proteins were identified as FGB, APOE, and APCS using matrix-assisted laser desorption ionization time of flight/mass spectrometry (Supplemental Table 6). Although most protein spots remained unchanged in 3 cases, high levels of 3 plasma proteins were identified in the lysate of eBVs compared with those of native valves. On the basis of our previous finding, fibrinogen and PLG, which are known as activators of macrophages,[14-17] accumulated in an eBV case,[8] and considering that APOE and APCS are known circulating proteins, it was essential to investigate their functional role in the implanted BV leaflets. Therefore, we performed additional quantitative investigations using multiple samples of tissue lysates from normal, explanted, and AS valves. As expected, western blot data showed that these 4 proteins were significantly up-regulated in tissue valves compared with normal valves (**Figures 3B and 3C**). Significantly high levels of fibrinogen, APCS, and APOE were observed in lysates from tissue valves compared with lysates of stenotic native valves (**Figures 3B and 3C**). Immunohistochemical staining of the identified proteins showed that the entire leaflet of the eBVs was strongly stained, although those of the preimplanted BVs and native normal valves were not stained (**Figure 4A**). Notably, brown colors derived from FGB and PLG were strongly detected around the calcified areas (**Figure 4A**, arrowheads). Further immunofluorescence investigations revealed that CD68-positive macrophages are usually found in interstitial areas with fibrinogen and PLG deposition (**Figure 4B**). Next, to confirm whether circulating components accumulated in the interstitium in the

FIGURE 3 Continued

(A) Two-dimensional gel electrophoresis of tissue lysates from native and bioprosthetic valves. The **left panels** are the enlarged figures of the areas surrounded by black broken lines in the **right panels**. **(B)** Western blot analyses for fibrinogen, plasminogen (PLG), apolipoprotein E (APOE), and anti-serum amyloid P component (APCS) in tissue lysates from the explanted native and bioprosthetic valves. **(C)** Statistical quantifications of the western blot results are presented. Analysis of variance, followed by Tukey's multiple-comparisons test (all comparisons), was used for statistical analyses of the fibrinogen, APCS, and APOE levels. The Kruskal-Wallis test (all comparisons) was used for statistical analyses of PLG levels. *$P < 0.05$ and ***$P < 0.001$. FGB = fibrinogen β-chain; other abbreviations as in **Figure 1**.

FIGURE 4 **Tissue Localization of Fibrinogen, PLG, Anti-APOE, and Anti-APCS**

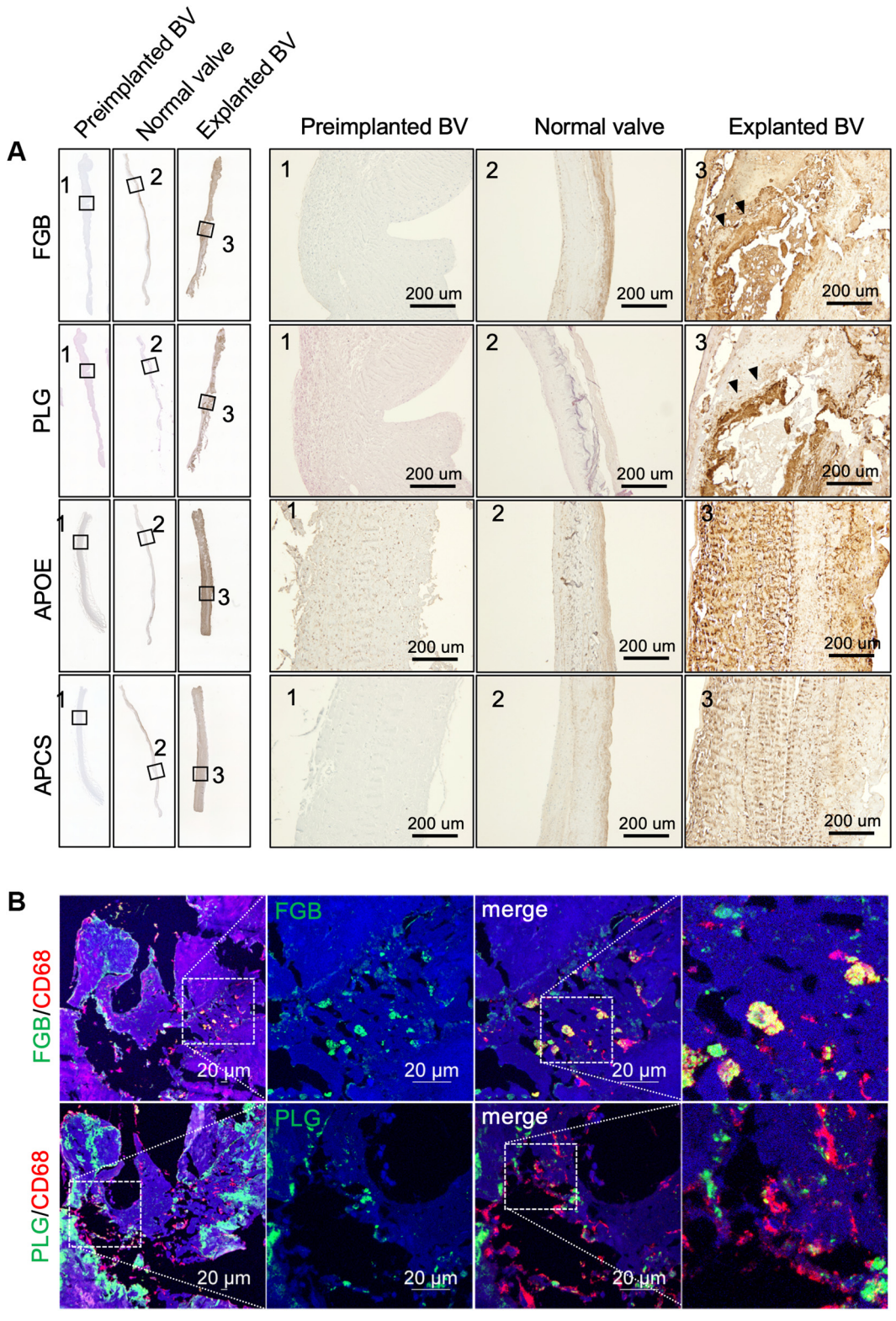

Continued on the next page

early stages after implantation, we histologically analyzed eBV leaflets obtained from a patient who died within 1 month after AVR. Remarkably, although no significant deterioration was noticeable (Supplemental Figure 6a), considerable collagen erosion, red blood cell infiltration, fibrinogen accumulation, and CD68-positive macrophage invasion into the interstitium were histologically observed in both the left ventricular and aortic sides (Supplemental Figure 6b).

To determine the functional roles of FGB, PLG, APOE, and APCS in macrophage behavior, we stimulated a human monocytic leukemia cell line (THP-1) by fibrinogen only or mixtures of fibrinogen, PLG, APOE, and APCS. The number of adhered THP-1 cells significantly increased on stimulations of fibrinogen or the protein mixtures, as there was no difference between the fibrinogen or protein mixtures (**Figures 5A and 5B**). To explain these phenotypes, we conducted RNA sequencing from vehicle-, fibrinogen-, or the mixture-treated THP-1 cells. Scatterplots show up-regulations of marker genes of activated macrophages, such as interleukin-6, chemokine (C-C motif) ligand 1, matrix metalloprotease 9, colony stimulating factor 1, chemokine (C-C motif) ligand 2, and interleukin-1B in the fibrinogen-treated THP-1 cells, while there were limited changes between fibrinogen only and mixtures of the 4 proteins (**Figure 5C**). Ingenuity Pathway Analysis signal pathway analysis showed that activations of interleukin and tumor necrosis factor signal cascade and differentiation and development of mononuclear leukocytes (**Figure 5D**). Canonical pathway exhibited that genes regarding agranulocyte and granulocyte adhesion as well as diapedesis were significantly enriched in the fibrinogen-stimulated THP-1 cells (**Figure 5E**, Supplemental Figure 7). The messenger RNA levels of the enriched genes were confirmed using quantitative polymerase chain reaction (**Figure 5F**). Additionally, to clarify the concentration dependency of 4 proteins in the macrophage activation, THP-1 cells were treated by each protein at various concentration around blood concentration as reported (Plasma Proteome Database). Interestingly, we found that fibrinogen and PLG accelerated macrophage activation at lower and higher concentrations, respectively, whereas macrophages were not activated by APOE and APCS treatment (Supplemental Figure 8). These data indicated that fibrinogen and PLG activate monocytes for the acceleration of cell adhesion and cytokine production.

EXPERIMENTAL EVALUATIONS OF VALVE DEGENERATION USING GOAT MODELS. On the basis of clinical studies, we hypothesized that pericardium-derived BVs might structurally allow circulating components' infiltration, such as fibrinogen and activated macrophages, because of looser collagen density. To test this hypothesis, we implanted glutaraldehyde-treated autologous pericardium in the aortic position in goats (**Figure 6A**) and histologically analyzed the temporal changes in valve structures (**Figure 6B**). As expected, infiltration of erythrocytes and FGB accumulations were identified in the interstitial spaces of the explanted valves from the third month after implantation (**Figures 6B and 6C**). Localizations of vimentin-positive spindle-shaped fibroblasts and macrophages, which were also structurally and pathologically identified using hematoxylin and eosin staining, were also observed in the explanted normal and pericardium-derived valves, respectively (**Figure 6C**). To quantify the FGB and PLG deposition levels, we obtained native and explanted pericardium-derived valves that were implanted for 12 months (Supplemental Figure 9). Western blotting data indicated that FGB and PLG proteins were strongly detected in lysates from the explanted pericardium-derived valves, while both proteins were not detected in lysates from normal native valves and the preimplanted pericardium (**Figure 6D**). Next, we assumed that strengthening the collagen fibers in bioprosthesis might prevent the infiltration of erythrocytes and macrophages. We focused on in-body tissue architecture (IBTA)-derived leaflets (IBTA leaflets/Biosheet leaflets), which are collagenous tissues produced using a novel subcutaneous embedding technology and are superior to native aortic

FIGURE 4 Continued

(A) Whole-valve leaflet views of the immunohistochemical images of the preimplanted and explanted bioprosthetic valves (BVs) and normal valve **(left panels)**. Porcine-derived eBV6, which strongly detected fibrinogen and PLG by western blotting, was stained using antifibrinogen or PLG antibodies. Bovine-derived eBV5, which was strongly detected by APOE and APCS using western blotting, was stained using anti-APOE and APCS antibodies. Preimplanted porcine- and bovine-derived BVs were used according to immunohistochemical staining against each species. The **right panels** show high magnification of the areas surrounded by lines in the whole view of the **left panels**. Scale bars, 200 μm. **Arrowheads** indicate strongly stained areas. **(B)** Immunofluorescence costaining of fibrinogen/CD68 or PLG/CD68 in the BV. Scale bars, 20 μm. Abbreviations as in **Figures 1 to 3**.

FIGURE 5 Fibrinogen Promotes Cell Adhesion and Activation of Macrophages

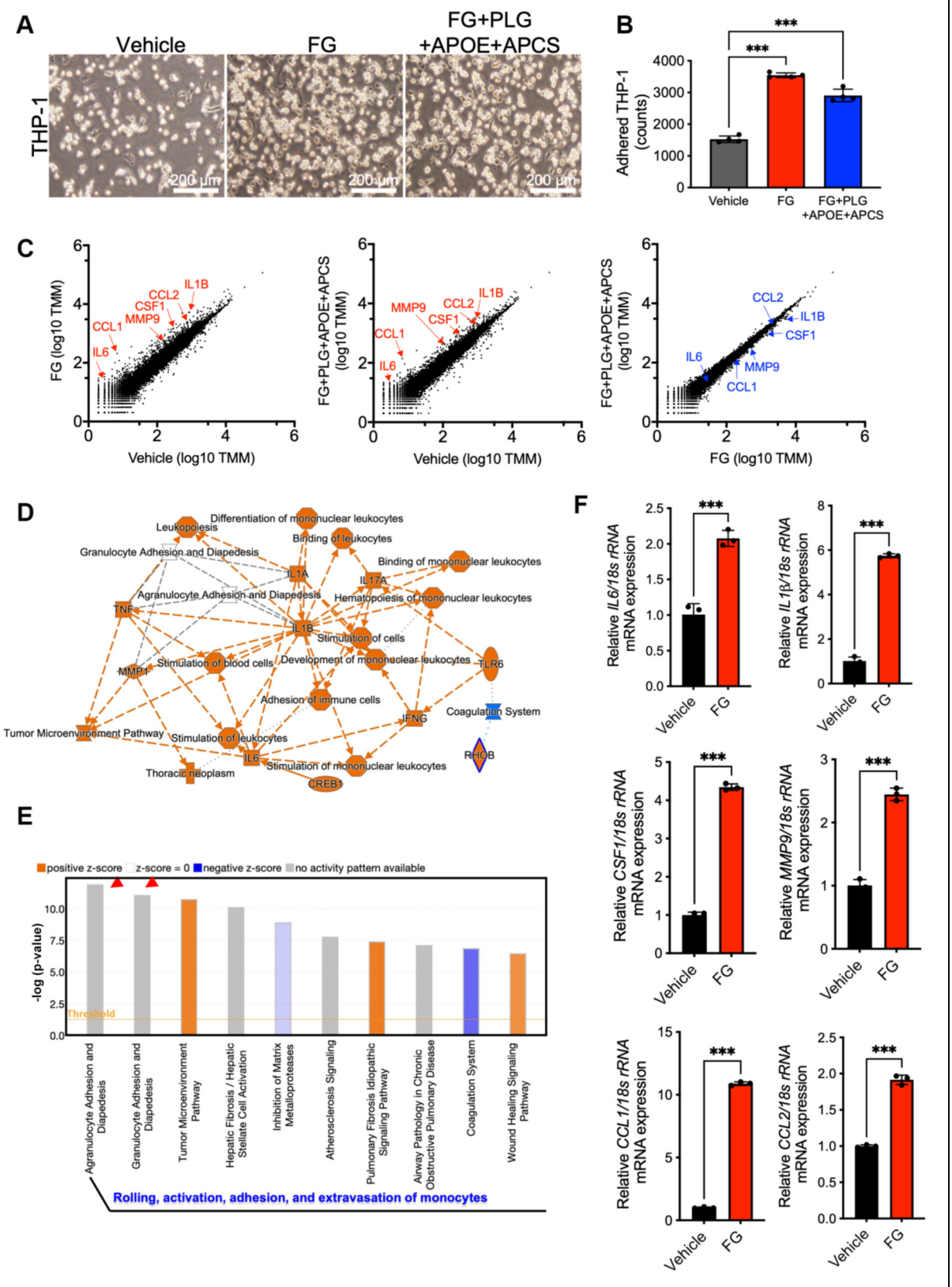

Continued on the next page

leaflets in physical strength.[18] We replaced the native aortic leaflets with IBTA leaflets in the aortic position and analyzed the histologic features of explanted IBTA valves at 3 and 12 months after implantation. The infiltrated red blood cells, FGB, and vimentin-positive macrophages were hardly detectable in the preimplanted and explanted IBTA valves (**Figures 7A and 7B**). We also found intact collagen fibers on the surface of IBTA valves, although there were numerous digested collagen fibers in the explanted pericardium-derived leaflets (**Figure 7C,** Supplemental Figure 10). The infiltration foci numbers and FGB accumulations significantly decreased in the IBTA leaflets compared with those of pericardium-derived bioprostheses, although both findings were not observed in normal native valve leaflets (**Figures 7D and 7E**). Our experimental data on animals confirm that the pericardium-derived BVs easily allow the infiltration of circulating components and strengthening the collagen fibers of the bioprosthesis effectively prevents structural valve degeneration (**Figure 7F**).

CATHEPSIN-POSITIVE APOPTOTIC MACROPHAGES IN CALCIFIED BVs. To explore the potential mechanism underlying the calcification of implanted tissue valves, we focused on 2 cases (porcine and bovine) of von Kossa staining-positive calcification and performed proteomics-based protein analyses using 2-dimensional gel electrophoresis. The obtained data were compared with the protein profile of non-calcified valves. We successfully identified CTSD using matrix-assisted laser desorption ionization time of flight/mass spectrometry analysis as a novel calcified tissue-specific protein (Supplemental Figures 11a and 11b, arrowheads; Supplemental Table 7). Immunohistochemical staining showed that CTSD-positive cells were rarely observed in noncalcified valves (Supplemental Figure 12a). Immunofluorescence costaining showed that CTSD was overexpressed in CD68-positive macrophages in tissue valves (Supplemental Figure 12b). We noted the overexpression of other cathepsins, such as cathepsin B, E, K, L, S, W, and Z, in CD68-positive macrophages around the calcified areas (Supplemental Figure 12c). Although low expression levels of cathepsin B and D were detected in the monocytes, both proteins were overproduced in the differentiated mature macrophages (Supplemental Figure 13). In contrast, although CD68-positive cells were also detected in the native normal valves and noncalcified BVs, cleaved caspase-3-positive apoptotic cells were rarely detected (**Figure 8A**). Further histologic investigation revealed that cleaved caspase-3 and CTSD double-positive macrophages were frequently observed around the von Kossa-positive calcified areas (**Figure 8A**). Numerous apoptotic macrophages were also detected by hematoxylin and eosin staining (**Figure 8B**), and these cells were mostly costained with anti-cleaved caspase-3 and CD68 antibodies (**Figure 8C**). Quantitative analyses revealed that CTSD-positive apoptotic macrophages were significantly accumulated in calcified compared with non-calcified eBVs (**Figure 8D**). Finally, to check whether strengthening collagen density can prevent cell apoptosis, we visualized and quantified apoptotic cells in the explanted pericardium-derived or IBTA valves using terminal deoxynucleotidyl transferase-mediated deoxyuridine triphosphate nick-end labeling staining. As shown in **Figure 8E**, although many apoptotic cells were observed in the interstitium of explanted pericardium-derived valves, the populations significantly decreased in the IBTA valves at 3 and 12 months after implantation (**Figure 8E**), suggesting that strengthening collagen densities for prevention of infiltration, activation by fibrinogen, and apoptosis of macrophages might have been effective for antideterioration therapy.

DISCUSSION

Combination of proteomic analyses and histologic investigations first uncovered excessive accumulations of CD68-positive macrophages and their activators, such as fibrinogen, in the interstitial space of implanted BVs, as well as the absence of CD34-positive fibroblastic interstitial cells, which are

FIGURE 5 Continued

(A) Bright-field images of vehicle-treated, fibrinogen (FG)–treated, and FG+PLG+APOE+APCS–treated adhered THP-1 cells on the culture dish. Scale bars, 200 μm. **(B)** Quantitative data of adhered THP-1 cells in **(A)**. Statistical analyses were performed using 1-way analysis of variance followed by Tukey's multiple-comparison test (all comparisons). ***$P < 0.001$. **(C)** Scatterplots for RNA sequencing datasets (vehicle vs FG, vehicle vs FG+PLG+APOE+APCS, and FG vs FG+PLG+APOE+APCS). **(D)** Graphical summary of the activated **(red)** and inactivated **(blue)** signal transduction from Ingenuity Pathway Analysis. **(E)** Top 10 enriched gene ontologies in canonical pathway database. **Arrowheads** indicate cell adhesion and diapedesis signaling of immune cells. **(F)** Quantifications of messenger RNA (mRNA) levels for genes regarding macrophage activations (unpaired *t*-test). ***$P < 0.001$. CCL = chemokine (C-C motif) ligand; CREB = cyclic adenosine 3',5'-monophosphate responsive element-binding protein; CSF = colony-stimulating factor; IL = interleukin; INFG = interferon gamma; MMP = matrix metalloprotease; RHOB = ras homolog family member B; rRNA = ribosomal ribonucleic acid; TLR = Toll-like receptor; TMM = trimmed mean of M values; TNF = tumor necrosis factor; other abbreviations as in **Figure 3**.

FIGURE 6 **Changes in the Implanted Pericardium-Derived Valves' Histologic Findings Using Goat Models**

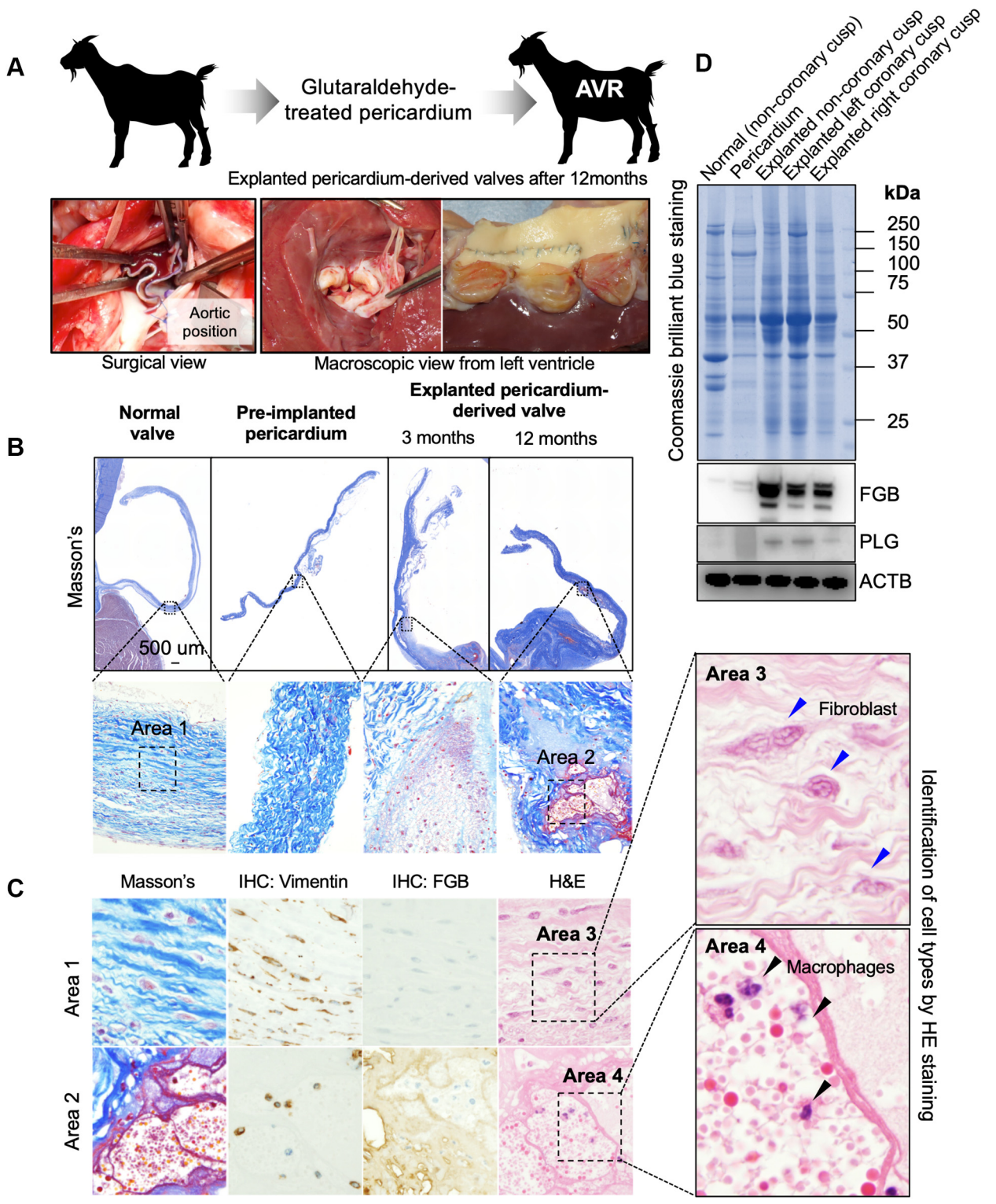

Continued on the next page

observed in the native valves (Figures 2 to 4). Our animal models reproduced human pathology regarding the infiltrations of circulating cells and proteins (Figure 6). Interestingly, further animal experiments successfully demonstrated that preventing infiltration by increasing collagen density and leaflet strength (Figures 7 and 8) is one of the solutions for antideterioration therapy.

Previous studies have revealed that valvular interstitial cells play essential roles in the maintenance of valve functions by providing an extracellular matrix under physiological conditions.[19] In a normal valve, valvular interstitial cells exist within 3 layers (fibrosa, spongiosa, and ventricularis) of the valve leaflet tissue (Figure 1). CD34-positive mesenchymal cells in the normal valves remarkably decreased by stenosis with calcification, although the CD34 levels were inversely related to α-SMA expression (Figures 2A and 2B). Although in the western blotting for α-SMA, a single band was detected in 1 case (eBV #9), no α-SMA-positive cells were observed in the entire leaflet from detailed histologic investigations, suggesting that invasions of smooth muscle actin-positive myofibroblasts followed by collagen synthesis might have barely occurred in the BVs. Previous studies have shown that CD34-positive cells were osteogenic endothelial progenitor cells, and they contributed to aortic valve calcification.[20,21] A recent study also revealed that isolated CD34-positive valve interstitial cells from the normal valves easily differentiated into osteoblastic cells.[22] Blaser et al[23] reported that transformation from fibroblastic valvular interstitial cells in the normal valves to myofibrogenesis for fibrosis and osteochondrogenesis for calcification largely contribute to the disease initiation and progression of AS. However, we found that CD34 was undetectable and CD68 was detectable mainly in lysates from eBVs (Figures 2A and 2B), suggesting that the molecular mechanisms of BV calcification were largely different from those of native valves, involving a transition of valve interstitial cells into osteoblasts. A recent study reported considerable infiltration of macrophages and erythrocytes in bioprosthetic heart valves using electron microscopy.[24] Our previous[8] and present findings suggest that the lack of valvular interstitial and endothelial cells and the pericardial tissue fragility may be linked to the deterioration of bioprosthetic aortic valves due to the infiltration of circulating components.

We successfully confirmed the phenotypes of fibrinogen and PLG accumulation on tissue valve leaflets from several patients (Figures 3 and 4). Luyendyk et al[14] suggested that fibrinogen and fibrinogen-related factors are scaffold proteins, which induce an acute inflammatory response to tissue damage via the activation of inflammatory cells such as leukocytes. Fibrinogen has been reported to promote immune responses by stimulating macrophages by binding to Toll-like receptor 4.[17] Moreover, it induces the expression of macrophage-produced cytokines, such as tumor necrosis factor, for the inflammatory response.[16] Hsieh et al[25] showed that fibrin and fibrinogen play different roles in macrophage activation. Our present data regarding RNA sequencing and gene enrichment analysis also demonstrate that fibrinogen promoted the activity of cell adhesion and induced cytokine production (Figure 5). Therefore, preventing the infiltration of circulating components, such as fibrinogen, might contribute to the prevention of macrophage adhesion and activation, which lead to valve calcification with cell death.

Although several proteomics analyses for native aortic valves have been conducted and researchers successfully identified biomarkers and therapeutic drug targets,[23,26] the present study is the first to report the performance of 2-dimensional gel electrophoresis for tissue lysates from explanted BVs. APOE is a member of the apolipoprotein family that functions as a ligand for low-density lipoprotein receptors, eliminating very low density lipoproteins.[27] Although the plasma apolipoprotein B/apolipoprotein A1 ratio was correlated with an increased risk for BV deterioration,[28] there was no evidence of the

FIGURE 6 Continued

(A) Schematic diagram of animal experiments using goats **(top)**. Surgical images of implantation procedure in the aorta **(bottom)**. **(B)** Masson's trichrome-stained whole-leaflet views of the normal valve and preimplanted and explanted pericardium-derived BVs (implantation term 3 and 12 months). **(C)** Masson's trichrome staining, hematoxylin and eosin (HE) staining, and immunohistochemistry (IHC) for vimentin and FGB of the areas (areas 1 and 2) surrounded by **broken lines** in the enlarged view of **(B)**. The **right panels** are high-magnification images of HE staining for identifications of cell types. **Blue and black arrowheads** indicate fibroblastic cells and macrophages, respectively. **(D)** A Coomassie brilliant blue image for the visualization of whole proteins and western blot images for the detection of FGB and PLG in tissue lysates from normal valves, pericardium, and explanted BVs. Blots of actin beta (ACTB) were used as an internal control. AVR = aortic valve replacement; other abbreviations as in Figures 3 and 4.

FIGURE 7 Histologic Evaluations of Explanted IBTA Valves

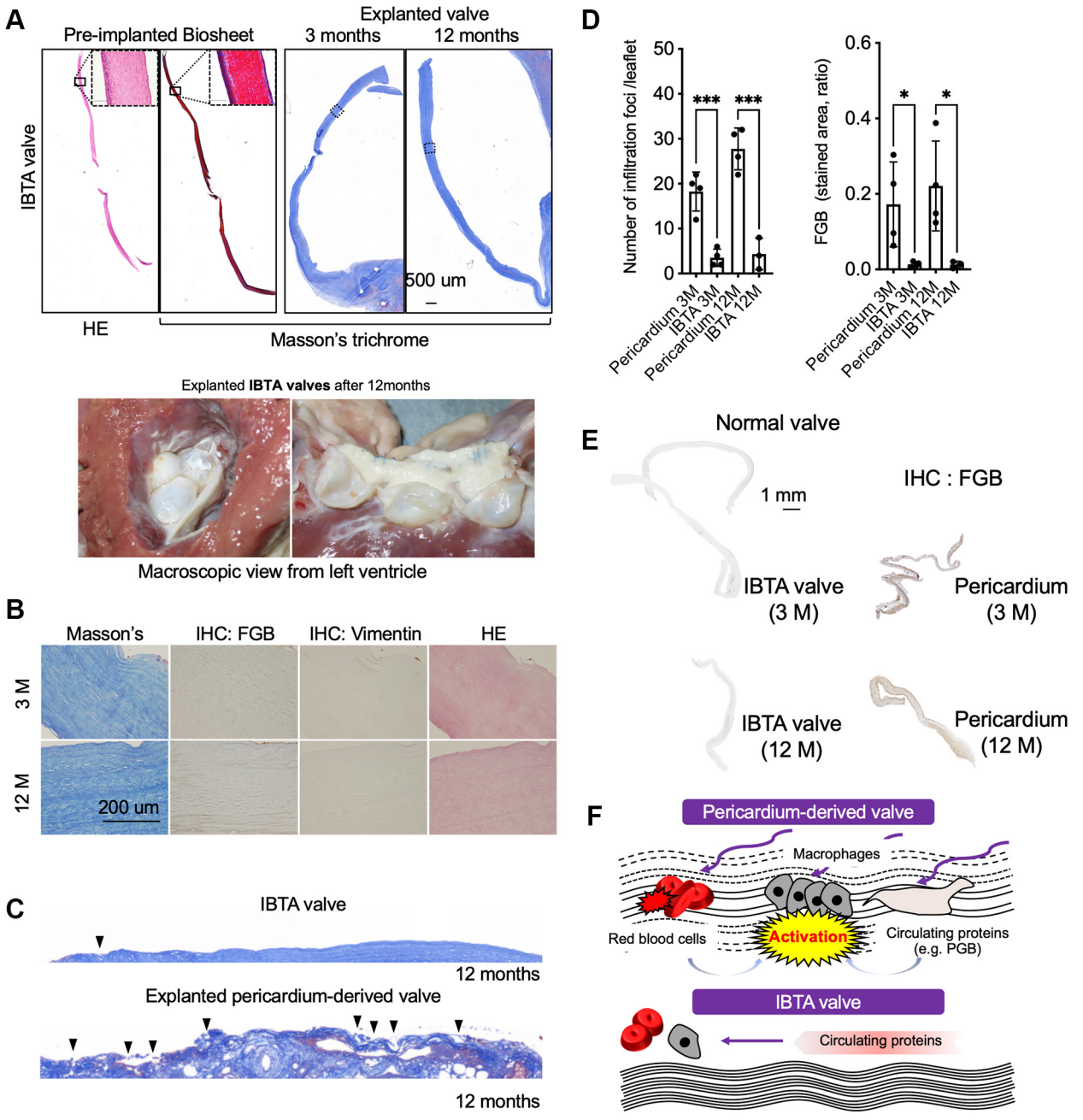

(A) HE- and Masson's trichrome–stained whole-leaflet views of the preimplanted Biosheet and explanted in-body tissue architecture (IBTA) valves (implantation term 3 and 12 months) **(top panel)**. Scale bars, 500 μm. Macroscopic views of the explanted valves **(bottom panel)**. **(B)** Masson's trichrome, HE, and IHC for vimentin and FGB of the areas surrounded by lines in the whole view of **right panels in A**. Scale bars, 200 μm. **(C)** Surface structures of Masson's trichrome–stained IBTA and pericardium-derived bioprosthetic valves for 12 months of implantation. **Arrowheads** indicate digested collagen fibers. **(D)** Quantifications of the infiltration foci per leaflet **(top panel)** and stained areas of immunohistochemistry against FGB **(bottom panel)**. Ratios were calculated by dividing brown-stained areas by the entire area of the leaflets. Statistical analysis was conducted using analysis of variance, followed by Sidak's multiple-comparisons test. **(E)** Whole-leaflet images of the explanted normal, IBTA (3 and 12 months), and pericardium-derived valves (3 and 12 months). All leaflets were immune stained with anti-FGB antibodies. Scale bar, 1 mm. **(F)** Schematic diagram of molecular mechanism regarding circulating proteins' and cells' infiltration. $*P < 0.05$ and $***P < 0.001$. PGB = plasminogen; other abbreviations as in Figures 3 and 6.

FIGURE 8 **Tissue Distributions of Cathepsin-Positive Apoptotic Macrophages**

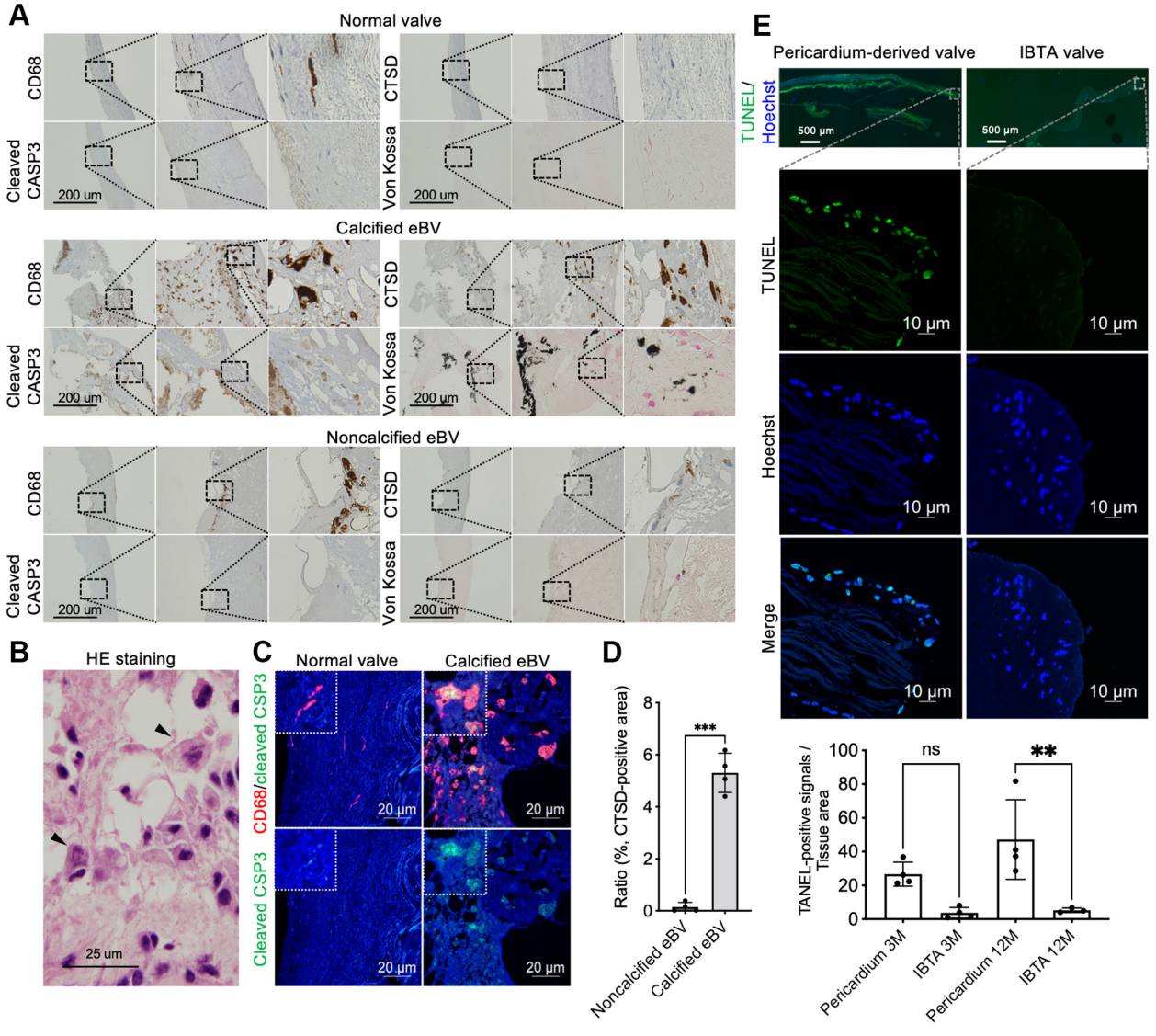

(A) Immunohistochemical staining of CD68, cleaved caspase-3 (CSP3), and cathepsin D (CTSD), as well as von Kossa staining in the normal **(top panels)**, calcified **(middle panels)**, and noncalcified **(bottom panels)** valves. **(B)** HE-stained image of apoptotic macrophages around the calcified bioprosthetic areas. **Arrows** indicate apoptotic macrophages. **(C)** Immunofluorescence costaining of CD68/cleaved caspase-3 in the bioprosthetic valves. Scale bars, 20 μm. **(D)** Quantifications of CTSD-positive areas in the noncalcified (n = 4) and calcified eBVs (n = 4) (unpaired *t*-test). **(E)** Representative images of apoptotic cells in the pericardium-derived and IBTA valves. The **top panels** depict whole views of terminal deoxynucleotidyl transferase-mediated deoxyuridine triphosphate nick-end labeling (TUNEL)–stained valves (green, TUNEL; blue; nucleus). The **middle panels** are high-magnification images of TUNEL staining in **top panel**. The **bottom panel** presents the quantitative data of fluorescence signals in the pericardium-derived (3 and 12 months) and IBTA (3 and 12 months) valves. Statistical analysis was conducted using analysis of variance, followed by Sidak's multiple-comparisons test. $^{**}P < 0.01$ and $^{***}P < 0.001$. Abbreviations as in Figures 1, 2, 6, and 7.

pathologic roles of tissue valve-associated APOE proteins, except for the fact that APOE deposited on tissues was associated with amyloidosis in Alzheimer's disease.[29] Previous combinations of proteomic and histologic analyses revealed that apolipoproteins, including APOE, colocated on the calcified areas of native valves.[26] However, there was no significant difference in the expression levels of APOE between AS and normal valves, whereas approximately 11-fold higher APOE levels were

detected in the tissue lysates from eBVs compared with those of normal valves (**Figure 3C**), suggesting that APOE can specifically bind to implanted bioprosthesis and might contribute to the degeneration of the BV. Conversely, amyloid deposition was reported in bioprosthetic cardiac valves[30] and induced valve calcification by promoting apoptosis of valvular interstitial cells.[31] Furthermore, APOE and APCS interact with amyloid fibers and promote amyloidosis.[32] Although APOE and APCS did not induce macrophage activation (**Figure 5,** Supplemental Figure 8), given the fact that lipoprotein-associated APOE and APCS are abnormally deposited onto xenograft aortic valves, both proteins may promote inflammation, amyloidosis, and calcification. In the future, functional analyses of the APOE and APCS using a xenograft animal model should be conducted.

CTSD messenger RNA was strongly induced by 7-beta-hydroxycholesterol, and this promoted the transformation of macrophages into foam cells, followed by apoptosis.[33] CTSD is essential for the apoptosis of macrophages via caspase-3 activation. Moreover, released cathepsins (other than CTSD) contribute to the degradation of the extracellular matrix during atherogenesis, and cathepsin L levels were correlated with the population of apoptotic macrophages.[34] Indeed, our RNA sequencing data indicated that the messenger RNA levels of cathepsin and matrix metalloprotease family genes in the macrophages were up-regulated by fibrinogen exposure (**Figure 5C**). Immunohistochemical staining indicated that overexpression of cathepsin family proteins, including CTSD, was observed in the CD68-positive macrophages located in the interstitium of explanted bioprosthesis (Supplemental Figure 12). These data suggest that infiltration of fibrinogen might directly induce the activation of macrophages and their transformation into cathepsin-positive foam cells, followed by their apoptosis via caspase-3 activation and degradation of collagen fibers of implanted bioprosthesis via induction of proteases production, such as cathepsin and matrix metalloproteases. In the future, further animal experiments using cathepsin gene-deleted goats should be conducted to examine whether cathepsins contribute to the apoptosis of accumulated macrophages.

The implantation of an autologous pericardium-derived bioprosthesis in goats clearly reproduced human pathologies, which involve the infiltration of macrophages and erythrocytes and circulating protein accumulation, suggesting that the degeneration of bioprostheses may be mainly induced by disruptions in pericardial tissues. To achieve more long-term durability, preventing infiltration by promoting endothelial coverage or strengthening the tissue density might be essential. Notably, a few infiltration foci and FGB accumulations were observed in IBTA valves, which had strengthened collagen densities and exhibited anticalcification phenotypes.[13] Iop et al[35] reported that decellularized allogeneic heart valves without glutaraldehyde treatments were appropriate for regenerating self-tissues containing vimentin-positive fibroblasts, α-SMA-positive myofibroblasts, and von Willebrand factor-positive endothelial cells. Moreover, IBTA technology-enabled tissue regeneration with the invasion of endothelial cells, mesenchymal cells, and strengthened collagen fibers resulted in the avoidance of calcification,[36,37] indicating that these technologies may enable the development of durable bioprostheses. Our data provide new insights into the development of antideterioration therapies for various BV implantations.

STUDY LIMITATIONS. Additional histological examinations of explanted various bioprosthetic valves derived from a larger number of patients will be required to confirm our conclusions. Further molecular identification using high-sensitivity proteomics with more in-depth quantifications will be needed to understand the entire molecular mechanism underlying structural valve degeneration. In vivo experiments should be conducted to examine whether cathepsins contribute to the calcification of bioprosthetic valves via induction of macrophage apoptosis.

CONCLUSIONS

Histological evaluations for explanted bioprosthetic valves identified the infiltration of macrophages and erythrocytes and circulating protein accumulation, which was reproduced by goat models and replaced with autologous pericardium-derived aortic valves. Further animal experiments concluded that strengthening the bioprosthesis leaflet's collagen fibers might be one of the solutions for preventing structural valve degeneration.

ACKNOWLEDGMENTS The authors thank Hirotomo Nakaoka, Isuzu Ikeuchi, Naohito Tokunaga, and Saki Fujii of the Advanced Research Support Center at Ehime University for their professional assistance, as

well as Dr Fujimasa Tada, Dr Kouki Watanabe, and Dr Hiroaki Miyaoka at Saiseikai Matsuyama Hospital for their support in obtaining autopsy samples.

FUNDING SUPPORT AND AUTHOR DISCLOSURES

This work was supported by Grants-in-Aid for Scientific Research (18K16396 to Dr Namiguchi, 16K10631, and 19H03740 to Dr Izutani, 19K17603 to Dr Hamaguchi, and 19K08585 and 16K109503 to Dr Aono) from the Ministry of Education, Culture, Sports, Science, and Technology of Japan; the Takeda Science Foundation (grants 2016 and 2020 to Dr Sakaue); the Public Trust Cardiovascular Research Foundation (grant 2017 to Dr Sakaue); the SENSHIN Medical Research Foundation (grant 2016 to Drs Aono and 2020 to Dr Sakaue); and the MSD Life Science Foundation, Public Interest Incorporated Foundation (grant 2016 to Dr Aono). Dr Nakayama is an employee of Biotube. There are no financial relationships between Dr Nakayama and the other coauthors, and experimental materials and funding used in this study were not provided by industry. All other authors have reported that they have no relationships relevant to the contents of this paper to disclose.

ADDRESS FOR CORRESPONDENCE: Dr Tomohisa Sakaue, Department of Cardiovascular Surgery, Ehime University Graduate School of Medicine, Shitsukawa, Toon City, Ehime 791-0295, Japan. E-mail: sakaue@m.ehime-u.ac.jp.

PERSPECTIVES

COMPETENCY IN MEDICAL KNOWLEDGE: Implantation of pericardium-derived bioprostheses, including transcatheter aortic valve replacement, is an excellent technique used worldwide for patients with AS with calcification. However, implanted BVs are occasionally explanted because of structural valve deterioration with calcification and thrombosis, which will increase in the future. Our findings regarding the accumulation of plasma proteins, such as fibrinogen and PLG, known activators of infiltrated macrophages from degenerated valve surfaces into interstitial spaces, are some of the cues explaining the mechanism of structural valve deterioration. Indeed, experiments using goats demonstrated that preventing infiltration by increasing collagen density and leaflet strength successfully suppressed the calcification of bioprostheses.

TRANSLATIONAL OUTLOOK: Our biochemical and animal experimental data will contribute to the development of next-generation bioprostheses without structural valve degeneration caused by calcification and thrombosis.

REFERENCES

1. Hammermeister K, Sethi GK, Henderson WG, Grover FL, Oprian C, Rahimtoola SH. Outcomes 15 years after valve replacement with a mechanical versus a bioprosthetic valve: final report of the Veterans Affairs randomized trial. *J Am Coll Cardiol*. 2000;36:1152–1258.

2. Bagur R, Pibarot P, Otto CM. Importance of the valve durability-life expectancy ratio in selection of a prosthetic aortic valve. *Heart*. 2017;103:1756–1759.

3. Roselli EE, Smedira NG, Blackstone EH. Failure modes of the Carpentier-Edwards pericardial bioprosthesis in the aortic position. *J Heart Valve Dis*. 2006;15:421–427.

4. McClure RS, Narayanasamy N, Wiegerinck E, et al. Late outcomes for aortic valve replacement with the Carpentier-Edwards pericardial bioprosthesis: up to 17-year follow-up in 1,000 patients. *Ann Thorac Surg*. 2010;89:1410–1416.

5. Johnston DR, Soltesz EG, Vakil N, et al. Long-term durability of bioprosthetic aortic valves: implications from 12,569 implants. *Ann Thorac Surg*. 2015;99:1239–1247.

6. Chakravarty T, Sondergaard L, Friedman J, et al. Subclinical leaflet thrombosis in surgical and transcatheter bioprosthetic aortic valves: an observational study. *Lancet*. 2017;389:2383–2392.

7. Sachdev S, Bardia N, Nguyen L, Omar B. Bioprosthetic valve thrombosis. *Cardiol Res*. 2018;9:335–342.

8. Sakaue T, Nakaoka H, Shikata F, et al. Biochemical and histological evidence of deteriorated bioprosthetic valve leaflets: the accumulation of fibrinogen and plasminogen. *Biol Open*. 2018;7:bio034009.

9. Frasca A, Xue Y, Kossar AP, et al. Glycation and serum albumin infiltration contribute to the structural degeneration of bioprosthetic heart valves. *J Am Coll Cardiol Basic Trans Science*. 2020;5:755–766.

10. Sakaue T, Shikata F, Utsunomiya K, et al. Proteomics-based analysis of lung injury-induced proteins in a mouse model of common bile duct ligation. *Surgery*. 2017;161:1525–1535.

11. Miura N, Takemori N, Kikugawa T, Tanji N, Higashiyama S, Yokoyama M. Adseverin: a novel cisplatin-resistant marker in the human bladder cancer cell line HT1376 identified by quantitative proteomic analysis. *Mol Oncol*. 2012;6:311–322.

12. Sakaue T, Sakakibara I, Uesugi T, et al. The CUL3-SPOP-DAXX axis is a novel regulator of VEGFR2 expression in vascular endothelial cells. *Sci Rep*. 2017;7:42845.

13. Kawashima T, Umeno T, Terazawa T, et al. Aortic valve neocuspidization with in-body tissue-engineered autologous membranes: preliminary results in a long-term goat model. *Interact Cardiovasc Thorac Surg*. 2021;32:969–977.

14. Luyendyk JP, Schoenecker JG, Flick MJ. The multifaceted role of fibrinogen in tissue injury and inflammation. *Blood*. 2019;133:511–520.

15. Cole HA, Ohba T, Nyman JS, et al. Fibrin accumulation secondary to loss of plasmin-mediated fibrinolysis drives inflammatory osteoporosis in mice. *Arthritis Rheumatol*. 2014;66:2222–2233.

16. Flick MJ, LaJeunesse CM, Talmage KE, et al. Fibrin(ogen) exacerbates inflammatory joint disease through a mechanism linked to the integrin alphaMbeta2 binding motif. *J Clin Invest*. 2007;117:3224–3235.

17. Smiley ST, King JA, Hancock WW. Fibrinogen stimulates macrophage chemokine secretion through toll-like receptor 4. *J Immunol*. 2001;167:2887–2894.

18. Terazawa T, Kawashima T, Umeno T, et al. Mechanical characterization of an in-body tissue-engineered autologous collagenous sheet for application as an aortic valve reconstruction material. *J Biomech*. 2020;99:109528.

19. Otto CM, Kuusisto J, Reichenbach DD, Gown AM, O'Brien KD. Characterization of the early lesion of 'degenerative' valvular aortic stenosis. Histological and immunohistochemical studies. *Circulation*. 1994;90:844–853.

20. Nomura A, Seya K, Yu Z, et al. CD34-negative mesenchymal stem-like cells may act as the cellular origin of human aortic valve calcification. *Biochem Biophys Res Commun*. 2013;440:780–785.

21. Gossl M, Khosla S, Zhang X, et al. Role of circulating osteogenic progenitor cells in calcific aortic stenosis. *J Am Coll Cardiol*. 2012;60:1945–1953.

22. Kanno K, Sakaue T, Hamaguchi M, et al. Hypoxic culture maintains cell growth of the primary

human valve interstitial cells with stemness. *Int J Mol Sci*. 2021;22:10534.

23. Blaser MC, Kraler S, Luscher TF, Aikawa E. Multi-omics approaches to define calcific aortic valve disease pathogenesis. *Circ Res*. 2021;128:1371–1397.

24. Kostyunin A, Mukhamadiyarov R, Glushkova T, et al. Ultrastructural pathology of atherosclerosis, calcific aortic valve disease, and bioprosthetic heart valve degeneration: commonalities and differences. *Int J Mol Sci*. 2020;21:7434.

25. Hsieh JY, Smith TD, Meli VS, Tran TN, Botvinick EL, Liu WF. Differential regulation of macrophage inflammatory activation by fibrin and fibrinogen. *Acta Biomater*. 2017;47:14–24.

26. Schlotter F, de Freitas RCC, Rogers MA, et al. ApoC-III is a novel inducer of calcification in human aortic valves. *J Biol Chem*. 2021;296:100193.

27. Mahley RW, Weisgraber KH, Huang Y. Apolipoprotein E: structure determines function, from atherosclerosis to Alzheimer's disease to AIDS. *J Lipid Res*. 2009;50:S183–S188.

28. Mahjoub H, Mathieu P, Senechal M, et al. ApoB/ApoA-I ratio is associated with increased risk of bioprosthetic valve degeneration. *J Am Coll Cardiol*. 2013;61:752–761.

29. Genin E, Hannequin D, Wallon D, et al. APOE and Alzheimer disease: a major gene with semi-dominant inheritance. *Mol Psychiatry*. 2011;16:903–907.

30. Goffin YA, Gruys E, Sorenson GD, Wellens F. Amyloid deposits in bioprosthetic cardiac valves after long-term implantation in man. A new localization of amyloidosis. *Am J Pathol*. 1984;114:431–442.

31. Audet A, Cote N, Couture C, et al. Amyloid substance within stenotic aortic valves promotes mineralization. *Histopathology*. 2012;61:610–619.

32. Pepys MB, Herbert J, Hutchinson WL, et al. Targeted pharmacological depletion of serum amyloid P component for treatment of human amyloidosis. *Nature*. 2002;417:254–259.

33. Li W, Yuan XM. Increased expression and translocation of lysosomal cathepsins contribute to macrophage apoptosis in atherogenesis. *Ann N Y Acad Sci*. 2004;1030:427–433.

34. Li W, Kornmark L, Jonasson L, Forssell C, Yuan XM. Cathepsin L is significantly associated with apoptosis and plaque destabilization in human atherosclerosis. *Atherosclerosis*. 2009;202:92–102.

35. Iop L, Bonetti A, Naso F, et al. Decellularized allogeneic heart valves demonstrate self-regeneration potential after a long-term preclinical evaluation. *PLoS ONE*. 2014;9:e99593.

36. Iwai R, Tsujinaka T, Nakayama Y. Preparation of Biotubes with vascular cells component by in vivo incubation using adipose-derived stromal cell-exuding multi-microporous molds. *J Artif Organs*. 2015;18:322–329.

37. Nakayama Y, Takewa Y, Sumikura H, et al. In-body tissue-engineered aortic valve (Biovalve type VII) architecture based on 3D printer molding. *J Biomed Mater Res Part B Appl Biomater*. 2015;103:1–11.

KEY WORDS bioprosthetic valve, calcification, macrophage, plasma protein, structural valve deterioration

APPENDIX For diagnostic definitions of diseases as well as supplemental tables and figures, please see the online version of this paper.